Tetrahedron 66 (2010) 9187–9193

Contents lists available at ScienceDirect

Tetrahedron

journal homepage: www.elsevier.com/locate/tet

The 1,3-dipolar cycloaddition of 1*H*-pyridinium-3-olate and 1-methylpyridinium-3-olate with methyl acrylate: a density functional theory study

Lydia Rhyman [a], Hassan H. Abdallah [b], Sabina Jhaumeer-Laulloo [a], Luis R. Domingo [c], John A. Joule [d], Ponnadurai Ramasami [a,*]

[a] *Department of Chemistry, University of Mauritius, Réduit, Mauritius*
[b] *School of Chemical Sciences, Universiti Sains Malaysia, 11800 Penang, Malaysia*
[c] *Departamento de Química Orgánica, Universidad de Valencia, Dr. Moliner 50, 46100 Burjassot, Valencia, Spain*
[d] *The School of Chemistry, The University of Manchester, Manchester M13 9PL, UK*

ARTICLE INFO

Article history:
Received 25 May 2010
Received in revised form 27 August 2010
Accepted 20 September 2010
Available online 24 September 2010

ABSTRACT

The 1,3-dipolar cycloaddition reaction of 1-substituted pyridinium 3-olates with methyl acrylate is studied using density functional theory (DFT) method at the B3LYP/6-31G(d) level. The molecular mechanisms of the possible stereo- and regio-chemical pathways are characterized and explored. Solvent effects are also evaluated by the polarizable continuum model (PCM). Analysis of the results shows that there are relevant differences in the reaction pathways between the gas phase and with solvent. Only results in solvent phase are in accord with literature experimental results where 6-substituted 8-azabicyclo[3.2.1]oct-3-en-2-ones are formed preferentially. These polar cycloaddition reactions take place through highly asynchronous transition states in which nucleophilic attack by C2/C6 of the pyridinium-3-olates on the more electrophilic centre of the methyl acrylate initiates the process. Analysis of global and local indexes of the reactants is evaluated in order to explain the observed regioselectivity. Rate constants are calculated at room temperature using conventional transition state theory.

1. Introduction

Cycloaddition reactions represent one of the most powerful processes in organic chemistry for the synthesis of cyclic and heterocyclic compounds due to their complete atom economy[1–3] and high functional group compatibility.[4] The usefulness of cycloaddition reactions arises from their versatility and stereoselectivity, allowing various types of carbocyclic structures to be constructed. 1,3-Dipolar cycloadditions (1,3-DCs), as first laid out by Huisgen in the early 1960s,[5] are the union of a 1,3-dipole with a dipolarophile to form a five-membered heterocyclic ring. This process is of great importance for general heterocyclic synthesis,[6] synthesis of complex natural products[7–9] and of bioactive molecules.[10] It is also an effective way of introducing new chiral centres attached to the heteroatoms.[11] Extensive experimental and theoretical studies have been carried out to understand the reaction mechanism and the origin of regiochemistry and stereochemistry in 1,3-DC reactions.[10]

1-Substituted pyridinium-3-olates, derived easily and simply from 3-hydroxypyridinium salts by *O*-deprotonation,[12] have been thoroughly investigated as dipoles and react with a variety of dipolarophiles.[13–17] One early driving force for studying these reactions was that the cycloadducts (CAs) have an 8-azabicyclo[3.2.1]octane skeleton as found in tropane alkaloids such as atropine, scopolamine and cocaine. Pioneering work by Katritzky and Takeuchi[13,14] identified *exo* and *endo* 8-azabicyclo[3.2.1]oct-3-en-2-one 6-esters on reaction of 1-methylpyridinium-3-olate with methyl acrylate and similar results were obtained[15] with 1-arylpyridinium-3-olates. More recently, careful analysis of several 1,3-DCs of pyridinium-3-olates showed that all four isomers are usually produced, but with the 6-substituted products predominating. For example, 1-methyl-4-phenylpyridinium-3-olate reacted with ethyl acrylate[16] giving a mixture of the 6-*exo* cycloadduct (for what comes later, we designate these isomers **CA6ex-R**, or **CA6en-R** where R defines the substituent on nitrogen), 6-*endo* (**CA6en**), 7-*exo* (**CA7ex**) and 7-*endo* (**CA7en**) isomers in a ratio of 33:26:20:12. In a study[17] of 1-methylpyridinium-3-olate itself with methyl acrylate, the **CA6ex**/**CA6en**/**CA7ex**/**CA7en** ratio was 5:4:4:0, however 7-*endo* isomers were formed using 1-benzylpyridinium-3-olate, the ratio being 4:4:2:1.

Pyridinium-3-olate cycloadditions were interpreted[12] by Katritzky et al. using valence bond and frontier molecular orbital (FMO) treatments. However, in order to have a better understanding, a detailed characterization of the various steps involved in the reaction sequence is required. This is difficult by experimentation alone and must rely on quantum mechanical computation, as the latter provides a direct tool for the understanding of organic

* Corresponding author. E-mail address: ramchemi@intnet.mu (P. Ramasami).

0040-4020/$ – see front matter © 2010 Elsevier Ltd. All rights reserved.
doi:10.1016/j.tet.2010.09.071

systems[18,19] and provides physical insight into the nature of transition states (TSs) and intermediates.[18,20]

Several theoretical studies have been devoted to 1,3-DC reactions,[21–23] however, for the reactions of pyridinium-3-olates, no theoretical studies have been reported. The 1,3-DC reactions of 1*H*-pyridinium-3-olate, **1a**, or 1-methylpyridinium-3-olate, **1b**, with methyl acrylate, **2**, can yield four isomeric CAs, the *endo* and *exo* stereoisomers from the two possible regiochemical pathways: 6-substituted products involve formation of bonds between the pyridinium C2 and ester C3 and pyridinium C6 and ester C2 while 7-substituted products have the opposite regiochemical orientation (Scheme 1). We have now studied these reactions theoretically, including kinetic studies. To the best of our knowledge, this is the first time that the rate constant of a 1,3-DC reaction has been evaluated theoretically.

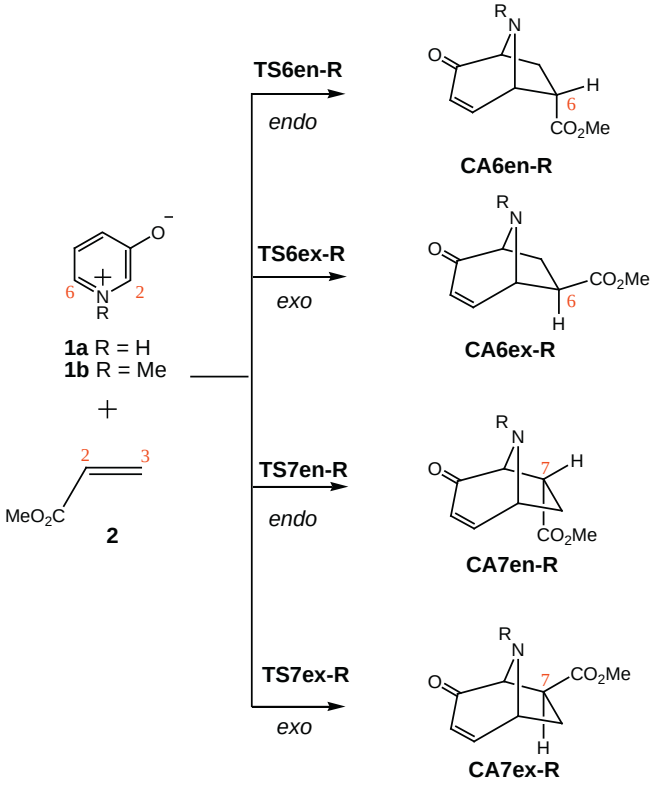

Scheme 1. Alternative pathways for the 1,3-DC reactions of 1-substituted pyridinium-3-olates **1a**,**b** with methyl acrylate **2**.

2. Computational methods

Density functional theory (DFT) has been used to optimize the molecular geometries using Becke's[24] three-parameter hybrid exchange (B3) with the Lee-Yang-Parr's[25] (LYP) correlation functional (B3LYP) in conjunction with 6-31G(d)[26] basis set. The B3LYP/6-31G (d) level has been shown to provide geometries and electronic properties in good correlation with reported experimental data.[27–29] Solvent effects were also taken into account in the framework of self-consistent reaction field (SCRF)[30,31] based on the polarizable continuum model (PCM) as developed by Tomasi's group.[32–34] The solvents used are tetrahydrofuran (THF) and ethanol at 298.15 K.[35] The relative energies were corrected for zero-point energies (ZPE) and the thermodynamic computations were scaled by a factor of 0.96.[36] The electronic structures of the critical points were studied by the natural bond orbital (NBO) method.[37,38]

The global electrophilicity index, ω, is given by the following simple expression,[39] $\omega=(\mu^2/2\eta)$, in terms of the electronic chemical potential μ and the chemical hardness η. Both quantities may be approached in terms of the one electron energies of the frontier molecular orbital HOMO and LUMO, ε_H and ε_L, as $\mu\approx(\varepsilon_H+\varepsilon_L)/2$ and $\eta\approx(\varepsilon_L-\varepsilon_H)$, respectively.[40,41] Recently, we have introduced an empirical (relative) nucleophilicity index, N based on the HOMO energies obtained within the Kohn–Sham scheme,[42] and defined as $N=E_{HOMO(Nu)}-E_{HOMO(TCE)}$. Tetracyanoethylene[43] (TCE) is chosen as reference as it presents the lowest HOMO energy in a large series of molecules already investigated in the context of polar cycloadditions. This choice allowed us conveniently to handle a nucleophilicity scale of positive values. Local electrophilicity[44] and nucleophilicity[45] indices, ω_k and N_k were evaluated using the following expressions: $\omega_k = \omega f_k^+$ and $N_k = N f_k^-$ where f_k^+ and f_k^- are the Fukui functions for a nucleophilic and electrophilic attacks, respectively.[46] All computations were carried out with the Gaussian 03 suite of programs.[47]

The rate constant was calculated at 298.15 K using conventional transition state theory (TST)[48–50] with the Wigner tunnelling coefficient.[48,51] According to the standard Eyring TST, the rate constant, *k*, is calculated as:

$$k = \Gamma \cdot \frac{k_B T}{h} \cdot \frac{Q_{TS} N_A}{Q_1 Q_2} \cdot e^{\left(\frac{-\Delta E_a}{RT}\right)} \quad (1)$$

where k_B is Boltzmann's constant; h is Planck's constant, T is the temperature; R is the ideal gas constant; N_A is the Avogadro's number; Q_{TS}, Q_1 and Q_2 are the total partition functions of TS, **1** and **2**, respectively; ΔE_a is the activation barrier for the cycloaddition reaction and Γ is the tunnelling coefficient.

3. Results and discussion

3.1. Energetics

Analysis of the stationary points involved in these 1,3-DC reactions indicates that these cycloadditions follow a one-step mechanism. Hence, four TSs, designated **TS6en-R**, **TS6ex-R**, **TS7en-R**, **TS7ex-R** and the corresponding CAs, **CA6en-R**, **CA6ex-R**, **CA7en-R**, **CA7ex-R**, where R signifies the substituent on nitrogen (H or Me) were located and characterized. Note, that in the channels leading

Table 1
Energies (*E*, in au) and relative energies[a] (ΔE, in kJ mol^{-1}) computed at 298.15 K and 1 atm in gas phase and solvents for the TSs and CAs involved in the 1,3-DC reactions of **1a** and **1b** with **2**

	Gas phase		THF		Ethanol	
	E	ΔE	*E*	ΔE	*E*	ΔE
1a	−323.3904	—	−323.4153	—	−323.4202	—
1b	−362.6758	—	−362.6941	—	−362.6975	—
2	−306.3746	—	−306.3805	—	−306.3816	—
TS6en-H	−629.7333	83.3	−629.7673	74.9	−629.7729	75.9
TS6ex-H	−629.7421	60.0	−629.7701	67.7	−629.7744	72.1
TS7en-H	−629.7303	91.0	−629.7631	86.1	−629.7684	87.9
TS7ex-H	−629.7383	70.1	−629.7664	77.2	−629.7713	80.1
TS6en-Me	−669.0188	82.9	−629.7701	68.8	−669.0522	70.5
TS6ex-Me	−669.0235	70.5	−629.7631	66.5	−669.0523	70.3
TS7en-Me	−669.0158	90.6	−669.0435	81.7	−669.0475	83.1
TS7ex-Me	−669.0198	80.4	−669.0458	75.5	−669.0495	77.6
CA6en-H	−629.7803	−40.3	−669.0489	−25.0	−629.8079	−15.9
CA6ex-H	−629.7535	−42.0	−669.0435	−26.7	−629.8088	−18.2
CA7en-H	−629.7802	−39.9	−669.2558	−22.7	−629.8072	−14.0
CA7ex-H	−629.7804	−40.4	−629.8047	−24.8	−629.8082	−16.5
CA6en-Me	−669.0617	−29.8	−629.8053	−25.1	−669.0863	−19.0
CA6ex-Me	−669.0603	−26.1	−669.0819	−21.0	−669.0852	−16.1
CA7en-Me	−669.0613	−28.7	−629.8046	−22.4	−669.0853	−16.4
CA7ex-Me	−669.0610	−27.8	−669.0838	−23.1	−669.0856	−17.1

[a] Relative to **1a**+**2** or **1b**+**2**.

to *endo* products, C3, C4 and C5 of the pyridinium ring overlay the ester group of methyl acrylate **2**, while for the *exo* products, only the nitrogen orbital could interact with the ester group. Table 1 shows the computed relative energies of the 1,3-DC reactions of the dipoles **1a** and **1b** with methyl acrylate **2** at 298.15 K and 1 atm in both gas phase and in the presence of a solvent.

The gas phase activation energies associated with these 1,3-DC reactions are 83.3 (**TS6en-H**), 60.0 (**TS6ex-H**), 91.0 (**TS7en-H**) and 70.1 (**TS7ex-H**) kJ mol^{-1} for the reaction of **1a** and 82.9 (**TS6en-Me**), 70.5 (**TS6ex-Me**), 90.6 (**TS7en-Me**) and 80.4 (**TS7ex-Me**) kJ mol^{-1} for the reaction of **1b**. In the gas phase, the *exo* approach mode is favoured over the *endo* mode by ca. 23.3 and 31.0 kJ mol^{-1} leading to the 6-substituted and 7-substituted CAs, respectively, for the reaction of dipole **1a** with methyl acrylate. Similarly, for the reaction of 1-methylpyridinium-3-olates **1b** with methyl acrylate, the *exo* pathway is more favoured than the *endo* pathway by ca. 12.4 kJ mol^{-1} leading to the 6-substituted CAs and by ca. 10.2 kJ mol^{-1} leading to the 7-substituted CAs. The gas phase energy differences between 6-*exo* and 7-*exo* (10.1 kJ mol^{-1}) and between 6-*endo* and 7-*endo* (7.8 kJ mol^{-1}) are too small to account for the regioselectivity reported in the literature, where 6-substituted 8-azabicyclo[3.2.1] oct-3-en-2-ones are preferred. All the 1,3-DC reactions studied proved to be exothermic by between −26.1 and −42.0 kJ mol^{-1}.

In the laboratory, these 1,3-DC reactions are carried out in polar solvents, and these can modify activation energies and selectivities, so the effects of THF and ethanol were considered. With the inclusion of solvent effects all species are stabilized, reactants being slightly more stabilized than TSs. As a result, the activation energies for all the cycloaddition processes in the polar solvents increase markedly. Interestingly, the *endo* TSs are more stabilized by the inclusion of solvent than the *exo* TSs, which correlates with the large dipole moments of the former (Table 4). In THF and ethanol, the channels leading to 6-esters are more favourable than those leading to 7-esters.

The activation energies for formation of 6-esters, in the two polar solvents, indicate that the *exo* approach is favoured over the *endo* approach; **TS6ex-H** and **TS6ex-Me** are lower in energy than **TS6en-H** and **TS6en-Me** by 7.2 and 2.4 kJ mol^{-1} in THF and by 3.8 and 0.3 kJ mol^{-1} in ethanol, respectively. Likewise, for the formation of 7-esters, the *exo* approach remains the more favourable pathway; **TS7ex-H** and **TS7ex-Me** are lower in energy than **TS7en-H** and **TS7en-Me** by 8.9 and 6.2 kJ mol^{-1} in THF and by 7.8 and 5.5 kJ mol^{-1} in ethanol, respectively. In addition, in these solvents **TS6en-Me** and **TS7en-Me** are slightly lower in energy than **TS6en-H** and **TS7en-H**, hence it can be concluded that substitution of a hydrogen atom by the methyl group on the nitrogen of 1-methylpyridinium-3-olate **1b** does not change the course of the reaction pathway. Significantly, the predicted activation energies are close to that obtained experimentally by Guiheneuf et al.,[35] which was carried out in ethanol for the 1,3-DC reaction of **1b** with **2**, 79.1 kJ mol^{-1}.

The thermodynamic parameters including activation enthalpies and activation Gibbs free energies as well as the reaction enthalpies and reaction Gibbs free energies at 298.15 K and 1 atm in THF and ethanol of the more favourable pathway are gathered in Table 2. The computed activation enthalpies range from 63.4 to 70.8 kJ mol^{-1} for the 1,3-DC reaction of the dipole **1a** with methyl acrylate **2** in THF, while a range of 70.2–74.0 kJ mol^{-1} is observed for the reaction in ethanol. Likewise, the predicted activation enthalpies of the dipole **1b** with **2** range from 65.9 to 68.5 kJ mol^{-1} in THF and from 67.9 to 68.3 kJ mol^{-1} in ethanol. The predicted activation enthalpies of 1-methylpyridinium-3-olate **1b** to methyl acrylate **2** are in fair agreement with the experimental value, 77.4 kJ mol^{-1} obtained in ethanol.[35] It is interesting to note that the activation enthalpy for the *exo* approach is lower compared to the *endo* approach. Moreover, the activation entropy corresponding to the *exo* approach is more negative than that corresponding to the *endo* approach. As a consequence, the activation free energies for formation of the **CA6ex** and **CA7ex** are lower than that for the **CA6en** and **CA7en**.

Table 2
Relative enthalpies (ΔH, in kJ mol^{-1}), free energies (ΔG, in kJ mol^{-1}) and entropies (ΔS, in J mol^{-1}) computed at 298.15 K and 1 atm in solvents for the TSs and CAs involved in the 1,3-DC reactions

	THF			Ethanol		
	ΔH	ΔG	ΔS	ΔH	ΔG	ΔS
TS6en-H	70.8	127.8	−191.4	74.0	130.2	−188.5
TS6ex-H	63.4	120.8	−192.5	70.2	126.0	−187.4
TS7en-H	81.8	139.2	−192.4	86.1	140.3	−181.8
TS7ex-H	75.2	131.3	−188.2	78.1	134.2	−188.2
TS6en-Me	68.5	121.6	−178.1	68.3	127.0	−197.0
TS6ex-Me	65.9	120.4	−182.7	67.9	127.4	−199.7
TS7en-Me	80.1	134.5	−182.3	80.7	139.9	−198.6
TS7ex-Me	73.2	132.2	−198.1	75.3	134.7	−199.3
CA6en-H	−29.3	30.9	−201.7	−19.7	39.1	−197.3
CA6ex-H	−30.9	29.3	−202.0	−22.0	36.5	−196.2
CA7en-H	−26.9	32.8	−200.2	−17.8	41.2	−198.0
CA7ex-H	−29.0	30.5	−199.5	−20.3	38.1	−195.8
CA6en-Me	−27.7	30.7	−195.7	−23.4	40.1	−213.0
CA6ex-Me	−25.2	37.4	−210.1	−20.4	43.2	−213.5
CA7en-Me	−24.9	33.6	−196.2	−20.8	42.8	−213.4
CA7ex-Me	−25.6	32.6	−195.3	−21.5	42.1	−213.4

In summary, we find that all the 1,3-DC reactions are exothermic processes and the **CA6ex** is slightly more stable than the **CA6en**. Moreover, from kinetic and thermodynamic points of view, the results suggest that the pathway leading to the **CA6ex** is preferred. Thus, the experimental observations that mixtures of four products are normally obtained, but with the 6-esters predominating and 6-*exo* and 6-*endo* formed in similar amounts,[12,16,17] are supported by the computations, where a small energy difference between the *endo* and *exo* CAs is observed.

3.2. Geometrical parameters

The geometries of the TSs are shown in Fig. 1a,b, while the lengths of the C–C forming bond involved in these 1,3-DC reactions are given in Table 3. An analysis of the lengths of the two forming bonds at the TSs shows that they are not formed to the same extent. It is also seen that the C3–C2 and C3–C6 forming bonds at the regioisomeric TSs are shorter than the C2–C6 and C2–C2 bonds, respectively. This suggests that the C–C bond formation to the more electrophilic conjugated C3 of methyl acrylate **2** is more advanced than that to C2. Hence, these 1,3-DC reactions take place via asynchronous TSs.

In the gas phase, the distance between the acidic N–H hydrogen atom of the dipole **1a** and the carbonyl oxygen atom of methyl acrylate at the most favourable **TS6ex-H** is 2.221 Å. This distance, showing an H–O hydrogen bond interaction in the TS, accounts for the large stabilization of **TS6ex-H** relative to **TS6en-H**;**TS6ex-H** is located 23.3 kJ mol^{-1} below **TS6en-H** (Table 1). This large gas phase stabilization disappears in ethanol, and as a consequence, the energy difference between the two TSs decreases to 3.8 kJ mol^{-1}. Inclusion of solvent effects causes a shortening of the forming bonds at C3 of methyl acrylate, while the lengths of the forming bonds at C2 are increased. Thus, in polar solvents, the TSs are slightly more advanced and more asynchronous.

The extent of the asynchronicity can be measured by considering the difference between the lengths of the two forming bonds at the TSs such that $\Delta d_6=[d(\text{C2–C6})-d(\text{C3–C2})]$ for 6-ester pathways and $\Delta d_7=[d(\text{C2–C2})-d(\text{C3–C6})]$ for 7-ester pathways. Table 3 reports the asynchronicity degrees, Δd in both gas phase and solvents. The *endo* TSs are more asynchronous than the *exo* TSs, and the more favourable TSs leading to 6-esters are more asynchronous compared to those leading to 7-esters. Inclusion of solvent effects

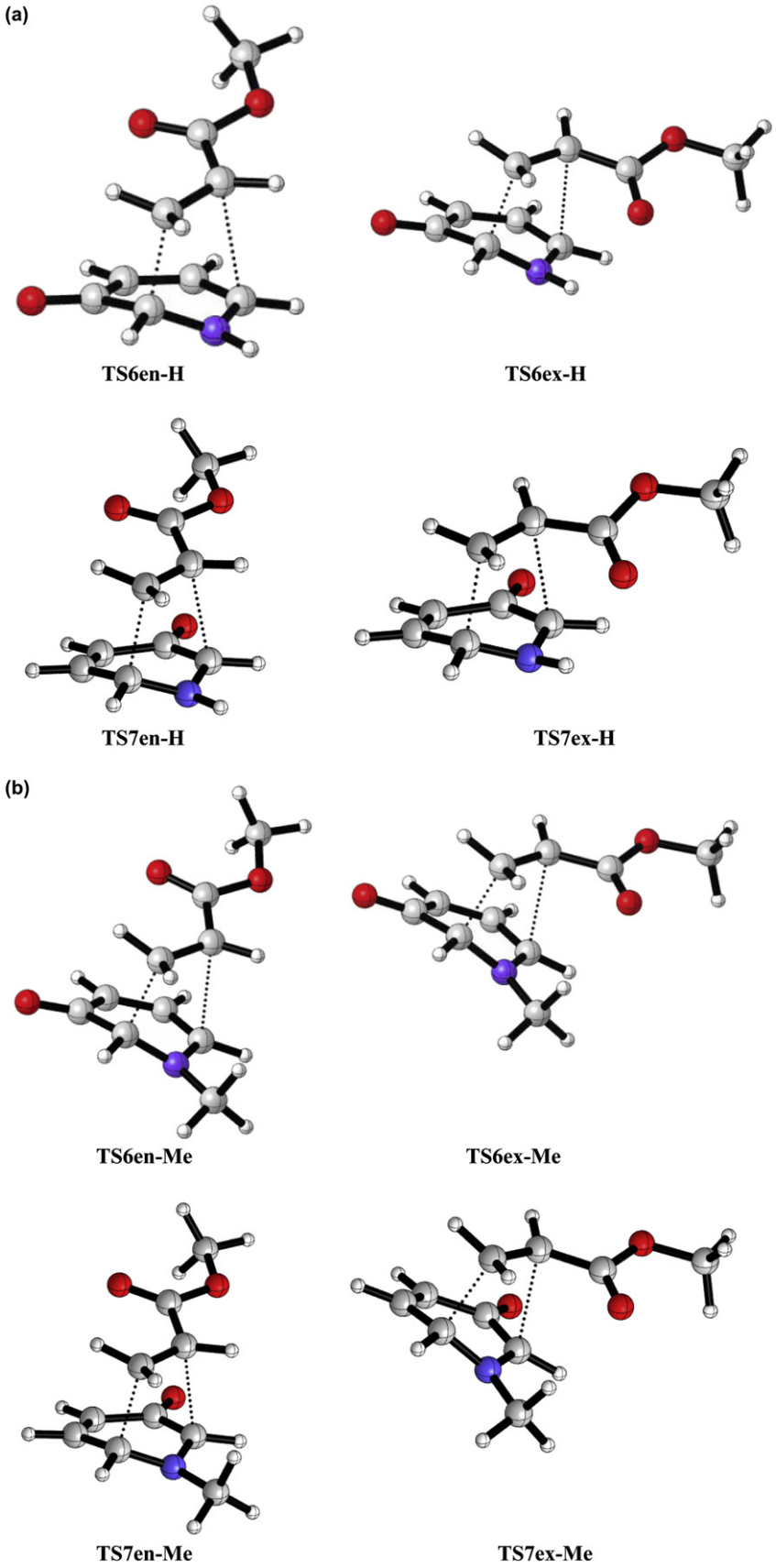

Fig. 1. (a) B3LYP/6-31G(d) optimized geometries of the TSs involved in the 1,3-DC reaction between 1*H*-pyridinium-3-olate **1a** and methyl acrylate **2**. (b) B3LYP/6-31G(d) optimized geometries of the TSs involved in the 1,3-DC reaction between 1-methylpyridinium-3-olate **1b** and methyl acrylate **2**.

Table 3
Bond lengths of the C–C forming bond (in Å) and asynchronicity, Δd, at the transition states

	C2–C6	C3–C2	Δd_6		C2–C2	C3–C6	Δd_7
Gas phase							
TS6en-H	2.718	1.979	0.74	**TS7en-H**	2.439	2.079	0.36
TS6ex-H	2.610	1.993	0.62	**TS7ex-H**	2.496	2.036	0.46
TS6en-Me	2.710	1.969	0.74	**TS7en-Me**	2.450	2.057	0.39
TSex-Me	2.669	1.947	0.72	**TS7ex-Me**	2.555	1.992	0.56
THF							
TS6en-H	2.790	1.888	0.90	**TS7en-H**	2.566	1.943	0.62
TSex-H	2.628	1.926	0.70	**TS7ex-H**	2.572	1.948	0.62
TS6en-Me	2.773	1.895	0.88	**TS7en-Me**	2.538	1.964	0.57
TS6ex-Me	2.684	1.903	0.78	**TS7ex-Me**	2.616	1.930	0.69
Ethanol							
TS6en-H	2.798	1.869	0.93	**TS7en-H**	2.590	1.918	0.67
TS6ex-H	2.639	1.909	0.73	**TS7ex-H**	2.589	1.929	0.66
TS6en-Me	2.787	1.880	0.91	**TS7en-Me**	2.554	1.948	0.61
TS6ex-Me	2.692	1.892	0.80	**TS7ex-Me**	2.634	1.917	0.72

Table 4
Charge transfer (CT, in e) and dipole moment (in Debye) of TSs

	Gas phase		THF		Ethanol	
	CT	Dipole Moment	CT	Dipole Moment	CT	Dipole Moment
TS6en-H	0.16	6.562	0.18	9.325	0.18	9.975
TS6ex-H	0.19	4.438	0.18	5.665	0.18	5.938
TS6en-Me	0.14	5.816	0.16	8.510	0.17	9.145
TS6ex-Me	0.18	3.811	0.19	5.967	0.20	6.468
TS7en-H	0.17	6.851	0.19	9.332	0.19	9.916
TS7ex-H	0.19	4.500	0.19	5.835	0.20	6.128
TS7en-Me	0.15	6.198	0.17	8.548	0.17	9.083
TS7ex-Me	0.19	4.512	0.20	6.066	0.21	6.406

causes an increase in the asynchronicity, which is related to the dielectric constant of the solvents. Moreover, a comparison of the Δd for the reaction of methyl acrylate with **1a** and **1b** in the gas phase and in solvents indicates that the Δd is larger with the dipole **1b** than with **1a** in the gas phase. However, in solvents, the *endo* TSs for **1a** have a larger asynchronicity compared to **1b**. Conversely, the *exo* TSs for **1b** have higher Δd than the *exo* TSs of **1a**, which may correspond to the electron-releasing ability of the *N*-methyl group of **1b**. Thus, we can conclude that the presence of the methyl group leads to a more asynchronous *exo* TS.

3.3. Bond order and charge analysis

The extent on bond-formation at the TSs is provided by the bond order (BO). The Wiberg bond indices[52] were computed using the NBO analysis as implemented in Gaussian 03. The BO values of the two C–C forming bonds are reported in Table S1. The BO values for the C3–C2 and C3–C6 bonds being formed at the regioisomeric TSs have larger values than the C2–C6 and C2–C2 bonds, respectively. However, the polar character of the solvents increases the BO values of the C–C forming bond at the conjugated C3 of methyl acrylate, and decreases the BO values of the C–C forming bond at C2, i.e., in solution the TSs are slightly more advanced and more asynchronous.

The electronic nature of these 1,3-DC reactions was also evaluated by analyzing the charge transfer (CT) at the TSs. The natural atomic charges at the TSs were shared between the dipoles **1a**,**b** and methyl acrylate fragments and these data are reported in Table 4. In the gas phase, the CT at the TSs, which fluxes from the dipoles to the methyl acrylate fragment, ranges from 0.16 to 0.19 e, indicating the polar nature of the 1,3-DC reactions. For the *exo* TSs, the CT is slightly higher than for the *endo* ones. With the inclusion of solvent effects, the CT at the TSs slightly increases, a fact that is in agreement with a more advanced and more asynchronous character of the TSs.

Table 4 also reports the dipole moments of the TSs. The *endo* TSs are more polar than the *exo* TSs in spite of their larger CT. With the inclusion of solvent effects, the dipole moment of the TSs increases as a consequence of an increase of the CT. The greater polar character of the *endo* TSs than the *exo* TSs, measured by the dipole moments, accounts for the higher solvation of the former. This explains the changes of regioselectivity between the gas phase and in solvent results.

3.4. Analysis based on the reactivity indices at the ground state of reagents

Recent studies devoted to Diels–Alder[53] and 1,3-DC[54] reactions have shown that the analysis of the global and local indices defined within the context of conceptual DFT are powerful tool in understanding the behaviour of polar cycloadditions.[55] In Table 5, we report the static global properties, namely, electronic chemical potential μ, chemical hardness η, global electrophilicity ω and global nucleophilicity N indices of the pyridinium-3-olates **1a**,**b** and methyl acrylate **2**.

Table 5
Electronic chemical potential (μ, in au), chemical hardness (η, in au), global electrophilicity (ω, in eV) and global nucleophilicity (N, in eV) for **1a**,**b** and **2**

	μ	η	ω	N
2	−0.1586	0.2267	1.51	1.72
1a	−0.1215	0.1402	1.43	3.91
1b	−0.1181	0.1385	1.37	4.02

The electronic chemical potential of methyl acrylate **2**, μ=−0.1586 au, is lower than those for the pyridinium-3-olates, μ=−0.1215 (**1a**) and −0.1181 (**1b**) au, indicating thereby that along a polar cycloaddition pathway, the net CT will be from the pyridinium-3-olates **1a**,**b** to the electron-deficient component **2**, in clear agreement with the CT analysis performed at the TSs.

The electrophilicity power of methyl acrylate **2** is 1.51 eV, a value that falls in the range of strong electrophiles within the ω scale.[53] On the other hand, the pyridinium-3-olates also present a significant electrophilicity, ω=1.43 (**1a**) and 1.37 (**1b**) eV, being classified as moderate electrophiles within the ω scale.[53] In nucleophilicity, N, of the reagents, while methyl acrylate presents a low nucleophilicity, N=1.72 eV, the pyridinium-3-olates present a high nucleophilicity, N=3.91 (**1a**) and 4.02 (**1b**) eV, respectively, accordingly being classified as strong nucleophiles.[56] The methyl substitution on the nitrogen atom of **1b** slightly increases the nucleophilic character as a consequence of the electron-releasing character of the methyl group. The N values for the dipoles **1a** and **1b** account for the slightly lower activation energy in condensed phase found for **TS7ex-Me** than that for **TS7ex-H**. The analysis of the electronic chemical potentials as well as the global electrophilicity and nucleophilicity indices indicates that along a polar cycloaddition pathway methyl acrylate **2** will act as a good electrophile while the pyridinium-3-olates **1a**,**b** will act as good nucleophiles.

The local electrophilicity ω_k of **2** and the local nucleophilicity N_k of the pyridinium-3-olates **1a**,**b** were analyzed in order to predict the best electrophilic/nucleophilic interaction and, therefore, to explain the observed regioselectivity (see Table 6).[57,58] When **2** behaves as an electrophile, the most electrophilic site is the conjugated C3 position, ω_1=0.62 eV. For the pyridinium-3-olates **1a**,**b** behaving as nucleophiles the most nucleophilic site is the olate oxygen atom: N_O=1.38 eV for **1a** and N_O=1.42 eV for **1b**. Therefore,

Table 6
Local electrophilicity (ω_k, in eV) and local nucleophilicity (N_k, in eV) indices of **1a**,**b** and **2**

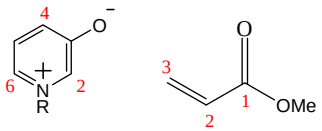

1a R = H
1b R = Me

2

		ω_k	N_k
2	3	0.62	0.02
	2	0.30	0.10
	1	0.30	0.08
	=O	0.23	1.29
1a	2	0.48	0.93
	6	0.19	0.81
	4	0.37	0.69
	O	0.01	1.38
1b	2	0.44	0.97
	6	0.18	0.83
	4	0.35	0.69
	O	0.01	1.42

the most favourable attack will be that associated with the conjugate addition of the olate oxygen atom of **1a**,**b** at C3 of **2**, i.e., an oxa-Michael-type addition. However, this would be readily reversible. Nucleophilic attack by C2 of **1a**,**b**, N_{C2}=0.93 eV at **1a** and N_{C2}=0.97 eV at **1b**, at the conjugated C3 position of **2** can be assisted by the concomitant ring closure with formation of the second bond, to yield the final CAs irreversibly. Significantly, it is found that for these 1,3-DC reactions, the C6 positions of the pyridinium-3-olates **1a**,**b** are also activated as nucleophilic centres: N_{C6}=0.81 eV for **1a** and N_{C6}=0.83 eV for **1b**. The greater nucleophilic activation at C2 than at C6 accounts for the regioselectivity experimentally observed in these polar cycloadditions of pyridinium-3-olates, and the lower activation energies computed for **TS6ex-R** relative to **TS7ex-R**.

3.5. Rate constant

The rate constants for the second order elementary step, denoted as k_1, were evaluated using conventional TST along with the Wigner transmission coefficient and are shown in Table S2. It turns out that **TS6ex-H** and **TS6ex-Me** have larger rate constants than **TS6en-H** and **TS6en-Me**. Moreover, the rate constant of **TS6ex-H** is hundred times higher than that of **TS6ex-Me** in the gas phase whereas in ethanol, the rate constant is only ten times higher. However, in THF, the rates of reaction are comparable for both **TS6ex-H** and **TS6ex-Me** due to comparable activation energies. Therefore, the faster reaction channels for the cycloadditions of both dipoles **1a** and **1b** with methyl acrylate **2** are those associated with formation of 6-ester products via *exo* approach. The rate constants from TS to the reactants, k_2, have also been calculated using the $\Delta G=-RT\ln K_{eq}$ and as $K_{eq}=k_1/k_2$, k_2 can also be calculated.

Experimentally, the overall rate constant for the 1,3-DC reaction of 1-methylpyridinium-3-olate **1b** to methyl acrylate **2** was determined by applying the Kezdy–Swinbourne method from the reactants to the CA.[59] The reported value is 0.345×10^{-3} cm^3 mol^{-1} s^{-1} while for the retrocycloaddition, the value is 1.4×10^{-6} s^{-1} at 29.8 °C and in ethanol as solvent.[35] The experimental rate constant cannot be compared with the predicted rate constant as the latter considers only the reactants-transition state elementary step. However, the calculated rate constant is sufficient to interpret the overall reaction.

4. Conclusions

DFT computation using B3LYP functional in conjunction with the 6-31G(d) basis set has been used to study the 1,3-DC reactions of 1*H*-pyridinium-3-olate **1a** and 1-methylpyridinium-3-olate **1b** to methyl acrylate **2**. These 1,3-DC reactions take place through an asynchronous TS associated with a one-step mechanism. Thermodynamic parameters, such as activation energies, enthalpy changes, entropy changes and Gibbs free energies of the possible *endo*/*exo* stereoisomeric and 6-ester/7-ester regioisomeric pathways have been determined. Solvent effects were also evaluated so as to mimic the experimental environment and it was found that results in solvent phase are in accord with literature experimental results where 6-substituted 8-azabicyclo [3.2.1]oct-3-en-2-one are preferred. Analysis of the global and local reactivity indices shows that these polar cycloadditions are characterized by a nucleophilic attack by C2 or C6 of the pyridinium-3-olates on the most electrophilic centre of the conjugated ester. The rate constants of the second order elementary step were calculated at room temperature using conventional TST. The findings of this research are in agreement with literature. This provides incentive to study the 1,3-DC of dipolarophiles with 1-substituted pyrazinium-3-olates and this will be the subject of a future report.

Acknowledgements

The authors acknowledge the comments from anonymous reviewers. Facilities from the Universiti Sains Malaysia and University of Mauritius are acknowledged. This work was supported by funding provided by the Tertiary Education Commission (TEC) of Mauritius. L.R.D. acknowledges research funds provided by the Ministerio de Ciencia e Innovación of the Spanish Government (project CTQ2009-11027/BQU).

Supplementary data

Supplementary data associated with this article can be found in the online version, at doi:10.1016/j.tet.2010.09.071.

References and notes

1. Aken, K. V.; Strekowski, L.; Patiny, L. *Beilstein J. Org. Chem.* **2006**, *2*.
2. Kumar, R. R.; Perumal, S. *Tetrahedron* **2007**, *63*, 7850–7857.
3. Kumar, R. R.; Perumal, S.; Manju, S. C.; Bhatt, P.; Yogeeswari, P.; Sriram, D. *Bioorg. Med. Chem. Lett.* **2009**, *19*, 3461–3465.
4. Wagner, G.; Danks, T. N.; Vullo, V. *Tetrahedron* **2007**, *63*, 5251–5260.
5. Huisgen, R. *Angew. Chem., Int. Ed. Engl.* **1963**, *2*, 565–598.
6. Padwa, A. *1,3-Dipolar Cycloaddition Chemistry*; Wiley-Interscience: New York, NY, 1984; Vols. 1–2.
7. Padwa, A. In *Synthetic Applications of 1,3-Dipolar Cycloaddition Chemistry toward Heterocycles and Natural Products*; Padwa, A., Pearson, A. W., Eds.; Wiley: Hoboken, 2003.
8. Merino, P., Chapter 13 In *Science of Synthesis*; Padwa, A., Ed.; George Thieme: New York, NY, 2004; Vol. 27, pp 511–580.
9. Desimoni, G.; Tacconi, G.; Barco, A.; Pollini, G. P. *Natural Products Synthesis through Pericyclic Reactions*; American Chemical Society: Washington, 1983.
10. Carruthers, W. *Cycloaddition Reactions in Organic Synthesis*; Pergamon: Oxford, 1990.
11. Gothelf, K. V.; Jørgensen, K. A. *Chem. Rev.* **1998**, *98*, 863–910.
12. Dennis, N.; Katritzky, A. R.; Takeuchi, Y. *Angew. Chem., Int. Ed. Engl.* **1976**, *15*, 1–9.
13. Katritzky, A. R.; Takeuchi, Y. *J. Chem. Soc.* **1970**, *92*, 4134–4136.
14. Katritzky, A. R.; Takeuchi, Y. *J. Chem. Soc. C* **1971**, 874–877.
15. Dennis, N.; Katritzky, A. R.; Matsuo, T.; Parton, S. K. *J. Chem. Soc., Perkin Trans. 1* **1973**, 746–750.
16. Kozikowski, A. P.; Araldi, G. L.; Ball, R. G. *J. Org. Chem.* **1997**, *62*, 503–509.
17. Estour, F.; Rézel, S.; Fraisse, D.; Métin, J.; Gaumet, V.; Lartigue, C.; Miscoria, G.; Gueiffier, A.; Blache, Y.; Teulade, J. C.; Chavignon, O. *Heterocycles* **1999**, *50*, 929–945.
18. Wiest, O.; Montiel, D. C.; Houk, K. N. *J. Phys. Chem. A* **1997**, *101*, 8378–8388.
19. Kuznetsov, M. L. *Russ. Chem. Rev.* **2006**, *75*, 935–960.
20. Klici, J. J.; Friesner, R. A. *J. Phys. Chem. A* **1999**, *103*, 1276–1282.
21. Türker, L.; Gümüş, S. *J. Comput. Theor. Nanosci.* **2009**, *6*, 873–879.

22. Benchouk, W.; Mekelleche, S. M.; Aurell, M. J.; Domingo, L. R. *Tetrahedron* **2009**, *65*, 4644–4651.
23. Xu, L.; Doubleday, C. E.; Houk, K. N. *J. Am. Chem. Soc.* **2010**, *132*, 3029–3037.
24. Becke, A. D. *J. Chem. Phys.* **1988**, *38*, 3098–3100.
25. Lee, C.; Yang, W.; Parr, R. G. *Phys. Rev. B* **1988**, *37*, 785–789.
26. Hehre, W. J.; Radom, L.; Schleyer, P. v. R.; Pople, J. A. *Ab Initio Molecular Orbital Theory*; Wiley: New York, NY, 1986.
27. Goldstein, E.; Beno, B.; Houk, K. N. *J. Am. Chem. Soc.* **1996**, *118*, 6036–6043.
28. Domingo, L. R.; Arńo, M.; Andrés, J. *J. Am. Chem. Soc.* **1998**, *120*, 1617–1618.
29. Garcia, J. I.; Martinéz-Merino, V.; Mayoral, J. A.; Salvatella, L. *J. Am. Chem. Soc.* **1998**, *120*, 2415–2420.
30. Tomasi, J.; Persico, M. *Chem. Rev.* **1994**, *94*, 2027–2094.
31. Simkin, B. Y.; Sheikhet, I. *Quantum Chemical and Statistical Theory of Solutions—A Computational Approach*; Ellis Horwood: London, 1995.
32. Cances, M. T.; Mennunci, V.; Tomasi, J. *J. Chem. Phys.* **1997**, *107*, 3032–3041.
33. Cossi, M.; Baronne, V.; Cammi, R.; Tomasi, J. *Chem. Phys. Lett.* **1996**, *255*, 327–355.
34. Baronne, V.; Cossi, M.; Tomasi, J. *J. Comput. Chem.* **1998**, *19*, 404–417.
35. Guiheneuf, G.; Laurence, C.; Katritzky, A. R. *J. Chem. Soc., Perkin Trans. 2* **1976**, 1829–1831.
36. Scott, A. P.; Radom, L. *J. Phys. Chem.* **1996**, *100*, 16502–16513.
37. Reed, A. E.; Weinstock, R. B.; Weinhold, F. *J. Chem. Phys.* **1985**, *83*, 735–746.
38. Reed, A. E.; Curtiss, L. A.; Weinhold, F. *Chem. Rev.* **1988**, *88*, 899–926.
39. Parr, R. G.; von Szentpaly, L.; Liu, S. *J. Am. Chem. Soc.* **1999**, *121*, 1922–1924.
40. Parr, R. G.; Pearson, R. G. *J. Am. Chem. Soc.* **1983**, *105*, 7512–7516.
41. Parr, R. G.; Yang, W. *Density Functional Theory of Atoms and Molecules*; Oxford University: New York, NY, 1989.
42. Kohn, W.; Sham, L. *J. Phys. Rev. A* **1965**, *140*, 1133–1138.
43. Domingo, L. R.; Chamorro, E.; Pérez, P. *J. Phys. Chem. A* **2008**, *73*, 4615–4624.
44. Domingo, L. R.; Aurell, M. J.; Pérez, P.; Contreras, R. *J. Phys. Chem. A* **2002**, *106*, 6871–6875.
45. Pérez, P.; Domingo, L. R.; Duque-Noreña, M.; Chamorro, E. *J. Mol. Struct. (THEOCHEM)* **2009**, *895*, 86–91.
46. Contreras, R.; Fuentealba, P.; Galván, M.; Pérez, P. *Chem. Phys. Lett.* **1999**, *304*, 405–413.
47. Frisch, M. J.; Trucks, G. W.; Schlegel, H. B.; Scuseria, G. E.; Robb, M. A.; Cheeseman, J. R.; Montgomery, J. A.; Vreven, T.; Kudin, K. N.; Burant, J. C.; Millam, J. M.; Iyengar, S. S.; Tomasi, J.; Barone, V.; Mennucci, B.; Cossi, M.; Scalmani, G.; Rega, N.; Petersson, G. A.; Nakatsuji, H.; Hada, M.; Ehara, M.; Toyota, K.; Fukuda, R.; Hasegawa, J.; Ishida, M.; Nakajima, T.; Honda, Y.; Kitao, O.; Nakai, H.; Klene, M.; Li, X.; Knox, J. E.; Hratchian, H. P.; Cross, J. B.; Adamo, C.; Jaramillo, J.; Gomperts, R.; Stratmann, R. E.; Yazyev, O.; Austin, A. J.; Cammi, R.; Pomelli, C.; Ochterski, J. W.; Ayala, P. Y.; Morokuma, K.; Voth, G. A.; Salvador, P.; Dannenberg, J. J.; Zakrzewski, V. G.; Dapprich, S.; Daniels, A. D.; Strain, M. C.; Farkas, O.; Malick, D. K.; Rabuck, A. D.; Raghavachari, K.; Foresman, J. B.; Ortiz, J. V.; Cui, Q.; Baboul, A. G.; Clifford, S.; Cioslowski, J.; Stefanov, B. B.; Liu, G.; Liashenko, A.; Piskorz, P.; Komaromi, I.; Martin, R. L.; Fox, D. J.; Keith, T.; Al-Laham, M. A.; Peng, C. Y.; Nanayakkara, A.; Challacombe, M.; Gill, P. M. W.; Johnson, B.; Chen, W.; Wong, M. W.; Gonzalez, C.; Pople, J. A. *Gaussian 03, Revision B04*; Gaussian: Wallingford, CT, 2004.
48. Truhlar, D. G.; Issacson, A. D.; Garett, B. C. *Generalized Transition State Theory* Vol. 4 of Theory of Chemical Reaction Dynamics, pp; CRC: Boca Raton, FL, 1985; 65–137.
49. Pilling, M. J.; Seakins, P. W. *Reaction Kinetics*, 2nd ed.; Oxford Science: Oxford, 1995.
50. Barreto, P. R. P.; Vilela, A. F. A.; Gargano, R. *Int. J. Quantum Chem.* **2005**, *103*, 685–694.
51. Wigner, E. P. Z. *Phys. Chem. B* **1932**, *19*, 203–216.
52. Wiberg, K. B. *Tetrahedron* **1968**, *24*, 1083–1096.
53. Domingo, L. R.; Aurell, M. J.; Pérez, P.; Contreras, R. *Tetrahedron* **2002**, *58*, 4417–4423.
54. Pérez, P.; Domingo, L. R.; Aurell, M. J.; Contreras, R. *Tetrahedron* **2003**, *59*, 3117–3125.
55. Domingo, L. R.; Sáez, J. A. *Org. Biomol. Chem.* **2009**, *7*, 3576–3583.
56. Jaramillo, P.; Domingo, L. R.; Chamorro, E.; Pérez, P. *J. Mol. Struct. (THEOCHEM)* **2008**, *865*, 68–72.
57. Domingo, L. R.; Chamorro, E.; Pérez, P. *Eur. J. Org. Chem.* **2009**, 3036–3044.
58. Bentabed-Ababsa, G.; Derdour, A.; Roisnel, T.; Sáez, J. A.; Pérez, P.; Chamorro, E.; Domingo, L. R.; Mongin, F. *J. Org. Chem.* **2009**, *74*, 2120–2133.
59. Swinbourne, E. S. *Analysis of Kinetic Data*; Nelson: London, 1971.